THE EFFECTS OF A PRIMORDIAL BLACK HOLE ON THE SURFACE OF A NEUTRON STAR

by

Brady Metherall

A dissertation submitted to the University of Ontario Institute of Technology in accordance with the requirements of the degree of Bachelor of Science (Hons) in the Faculty of Science

March 31, 2017

UNIVERSITY OF ONTARIO
INSTITUTE OF TECHNOLOGY

ABSTRACT

ACKNOWLEDGEMENTS

AUTHOR'S DECLARATION

I declare that the work in this thesis was carried out in accordance with the regulations of the University of Ontario Institute of Technology. The work is original except where indicated by special reference in the text and no part of the dissertation has been submitted for any other degree. Any views expressed in the dissertation are those of the author and in no way represent those of the University of Ontario Institute of Technology. The thesis has not been presented to any other University for examination either in Canada or elsewhere.

Brady Metherall
March 31, 2017

Contents

List of Figures

1. INTRODUCTION

A black hole is a region of space where enough mass is concentrated such that nothing, including light, cannot escape its gravitational pull. The effective radius of a black hole is called the Schwartzchild radius and can be derived from general relativity or the escape velocity and is given by

$$r_s = \frac{2Gm}{c^2}.$$

For example, in order for the Sun to become a black hole all of its mass would need to be compacted into a spherical region three kilometers in radius; and the Schwartzchild radius for the Earth is only nine millimeters.

The most common type of black holes are stellar black holes which form from the collapse of a massive star. Stellar black holes typically have masses between a few solar masses, and a few tens of solar masses. However, black holes can form by other mechanisms, and so have a very wide range of masses. It is presumed that at the centre of many galaxies lies a super massive black hole with a mass of hundreds of thousands, or even millions, of solar masses. And on the other extreme, black holes can have a mass considerably less than the Earth's. But since the density of a black hole is inversely proportional to its mass – these small mass black holes are unfathomably compact and dense. The only known possible mechanism to create such a dense object is from perturbations in the very early universe, and as such are

called primordial black holes.

1.1 Primordial Black Holes and Dark Matter

In astrophysics today, one of the least understood phenomena is dark matter, matter that does not interact with electromagnetic radiation, and is very hard to detect on Earth. Despite this, estimates suggest dark matter comprises approximately 25% of the mass in the universe, while the baryonic matter, the matter we can observe on Earth, is only around 5% [7, 21].

There are several theories for what the identity of dark matter is, and one candidate is primordial black holes. Primordial black holes are a viable candidate since they are neutrally charged, do not emit light, travel at non-relativistic speeds, and of course, have a significant mass.

Black holes slowly evapourate away through a process called Hawking radiation [15], and the time required for a black hole to entirely evapourate is

$$t_{ev} = \frac{5120\pi G^2 M_0^3}{\hbar c^4}.$$

Thus, lower mass black holes evapourate more quickly. In fact, primordial black holes with an initial mass around 10^{15}g would be exploding now as they vanish into nothing. By carefully looking for signs of a primordial black hole interaction with another massive object, the mass can be constrained, as well as the number density of primordial black holes. Which in turn can be used to estimate their contribution to dark matter.

1.2 Literature Review

Multiple groups have studied primordial black holes [4], and several constraints have been placed on their masses, as well as the conditions in the early universe when they may have formed. Since primordial black holes would have formed in the radiation-dominated era, the big bang nucleosynthesis constraint of baryonic matter comprising 5% of the critical density does not apply [7, 21]. Thus, primordial black holes are considered non-baryonic and are treated the same as all other cold dark matter. The properties mentioned earlier are useful because other theories need to make additions to the Standard Model, such as weakly interacting massive particles (WIMPs) like supersymmetric particles or axions [16]. Many theorists are becoming skeptical of these theories because of this [11].

Gravitational lensing has greatly constrained the viable mass ranges of primordial black holes. Several ranges of masses have been excluded: $10^{17} - 10^{20}$g by femtolensing of gamma-ray bursts [18], $10^{-3} - 60M_{\odot}$ by microlensing of quasars, and $10^{6} - 10^{9}M_{\odot}$ by millilensing of compact radio sources [23]. Furthermore, tidal disruption, and heating of galaxies constrains masses above $10^{5}M_{\odot}$ [5]. And as previously mentioned, primordial black holes smaller than about 10^{15}g have already completely evapourated. And it has been shown that the range from 10^{-7} to $10M_{\odot}$ is also excluded [22]. Leaving $10^{16} - 10^{17}$g, $10^{20} - 10^{26}$g, and $10 - 10^{5}M_{\odot}$ as the potential mass ranges of primordial black holes [2].

In the first half of this thesis we shall be reproducing the work done by Defillon, Granet, Tinyakov, and Tytgat [9] defined by the following model.

1.3 Model

In this thesis we use a relatively simplistic model for the collision of a primordial black hole and a neutron star. We shall treat the primordial black hole as a point mass, and the neutron star to be flat and infinite. This allows us to use cylindrical coordinates with no angular dependence. This is a reasonable approximation to make, given the sheer size difference between the primordial black hole and the neutron star. Although neutron stars are fairly compact, and very dense, primordial black holes are microscopic, and so the curvature of the neutron star is negligible compared to the primordial black hole. Also, we will be using the assumption that the velocity of the primordial black hole is constant. Despite the fact that the primordial black hole would be accelerating into the neutron star, this is a fair assumption to make. Most of the energy transfer occurs in a relatively short time, as we shall see in Section 3.4, during which we can approximate a constant velocity.

Furthermore, we will be using Newtonian gravity with the potential

$$\Phi = \frac{-Gm}{\sqrt{r^2 + (z + vt)^2}} \tag{1.1}$$

to greatly simplify the solution. Given the mass scales of neutron stars, and primordial black holes, general relativity would be more appropriate, however, it is too complicated.

Lastly, we will be modelling the neutron star as an incompressible, ideal fluid. This is a fairly common assumption in astrophysics because stars share many features with fluid dynamics. Stars are a continuous soup of particles, they have a free surface, and undergo convection and advection.

1.4 Outline

The rest of this thesis is organized as follows: Chapter 2 we will define the Hankel transform and derive some useful theorems and corollaries which will be of utmost importance; Chapter 3 we shall analytically calculate the energy transferred during the interaction. Then, in Chapter 4 we will use the same model and simulate the collision using PySPH, and finally in Chapter 5, we make conclusions.

2. OPERATORS AND INTEGRAL TRANSFORMS

Before starting the in-depth analysis, we first must introduce key definitions, and theorems, several of which have been modified from [14], to more easily analytically solve the velocity potential of the neutron star.

Definition 2.1 (Operator)**.** *Let A, and B be vector spaces with respective subspaces, X, and Y. An operator $\mathcal{T}$, maps any $x \in X$ to Y, and is denoted by $\mathcal{T}(x)$.*

Common examples of operators are the Sturm-Liouville operator, the Laplacian, or the Hamiltonian. Our focus will be on the integral operator, or transform.

Definition 2.2 (Integral Transform)**.** *Let the domain, and co-domain of the transform be $C[a,b]$[§] and $K : \mathbb{R}^2 \to \mathbb{R}$, then we can define our operator $\mathcal{T} : C[a,b] \to C[a,b]$ as*

$$(\mathcal{T}f)(x) = \int_a^b f(y)K(x,y)\,dy,$$

where K is called the kernel function.

[§] $C[a,b]$ denotes the set of continuous functions on the interval $[a,b]$. Likewise, $C^n[a,b]$ denotes the set of functions whose n-th derivative is continuous on the interval $[a,b]$.

During the analysis, a specific integral transform will be used, namely the Hankel transform, which will be defined shortly. Typically, the bounds of integral transforms are either 0 or $-\infty$, to ∞, and therefore, the following definition and theorem are necessary to show that integral transforms are well behaved, and continuous.

Definition 2.3 (Uniform Continuity)**.** *A function $f : X \to Y$, with $X, Y \subseteq \mathbb{R}$, is uniformly continuous if $\forall \varepsilon > 0$, $\exists\, \delta > 0 : |x - x_0| < \delta \Rightarrow |f(x) - f(x_0)| < \varepsilon$, $\forall x_0 \in X$.*

Uniform continuity has a very similar formal definition to continuity, the difference being of course, is that δ must be the same for the entire domain. Furthermore, continuity is only defined for a point, whereas uniform continuity is defined over an interval.

Theorem 2.4 (Heine-Cantor Theorem)**.** *If a function $f : X \to \mathbb{R}$, with X a closed, subset of the real numbers, is continuous, f is uniformly continuous on X.*

Proof. Since f is continuous, by Cousin's Theorem [6] there exists a finite subcover of X[§]:

$$\{B_{\delta_i/2}(x_i) : 1 \leq i \leq n \in \mathbb{N}\} : X \subseteq \bigcup_{i=1}^{n} B_{\delta_i/2}(x_i),$$

such that

$$\forall\, \frac{1}{2}\varepsilon > 0,\, \exists\, i : |x - x_i| < \frac{1}{2}\delta_i \Rightarrow |f(x) - f(x_i)| < \frac{1}{2}\varepsilon\, \forall\, x \in X.$$

Now, let $\delta = \min\{\frac{1}{2}\delta_i : 1 \leq i \leq n\}$, and suppose, $|x - x_0| < \delta$, then, $\exists i : |x - x_i| < \frac{1}{2}\delta_i$.

[§]Figure 2.1 helps visualize the concept of finite subcovers.

Then,

$$|x_0 - x_i| \leq |x_0 - x| + |x - x_i| < \delta + \frac{1}{2}\delta_i \leq \delta_i,$$
$$|f(x_0) - f(x)| \leq |f(x_0) - f(x_i)| + |f(x_i) - f(x)| < \frac{1}{2}\varepsilon + \frac{1}{2}\varepsilon = \varepsilon$$

by the triangle inequality. □

Physically, we require the velocity potential to be continuous, and so the Hankel transform (and in fact all integral transforms) should preserve continuity, as shown in Theorem 2.5.

Theorem 2.5. *$\mathcal{T}f$ is continuous if $\int_a^b |f(y)|dy < \infty$, and $K(x, y)$ is uniformly continuous on $[a, b]$.*

Proof. For all $\varepsilon > 0$, choose $\delta : |x - x_0| < \delta$, so that $|K(x, y) - K(x_0, y)| < \varepsilon/M$, with $M = \int_a^b |f(y)|dy$. Then,

$$\begin{aligned}
|(\mathcal{T}f)(x) - (\mathcal{T}f)(x_0)| &= \left| \int_a^b K(x, y)f(y)dy - \int_a^b K(x_0, y)f(y)dy \right| \\
&\leq \int_a^b |K(x, y) - K(x_0, y)||f(y)|dy \\
&< \int_a^b \frac{\varepsilon}{M}|f(y)|dy \\
&< \varepsilon,
\end{aligned}$$

and $\mathcal{T}f$ is continuous. □

The conditions for Theorem 2.5 are automatically satisfied by Theorem 2.4 if a and b are finite, and K is bounded and continuous.

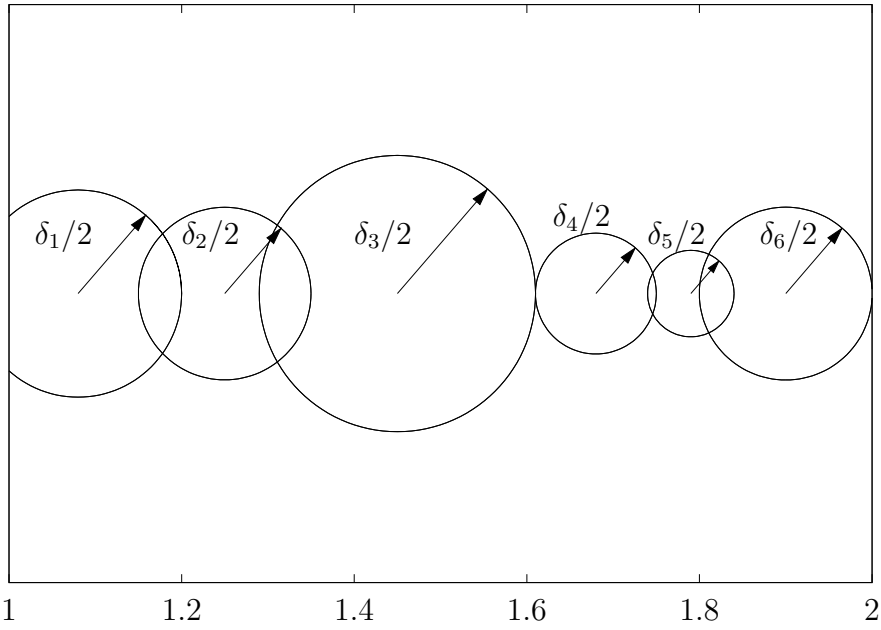

Figure 2.1: Cousin's Theorem states that there exists a finite subcover of a closed interval. For example, consider the interval $[1, 2] \in \mathbb{R}$, then there exists a finite collection of circles (or more generally balls) of radii $\delta_i/2$ which spans the interval.

2.1 Hankel Transform

The Hankel transform, named after the German mathematician Hermann Hankel, is quite common in cylindrically symmetric systems, such as ours, and arises from the eigenfunctions of Laplace's equation.

Definition 2.6 (Hankel Transform)**.** *The Hankel transform of a function $f(s)$ is given by*

$$(\mathscr{H}_\nu f)(\sigma) = \int_0^\infty f(s) J_\nu(s\sigma) s \, ds,$$

where J_ν is the Bessel function of the first kind, of order $\nu \geq -\frac{1}{2}$, and σ is a non-negative real variable.

Notice too, that it directly follows from Definition 2.6 that the Hankel transform is self-reciprocal.

Corollary 2.7 (Inverse Hankel Transform)**.** *The Hankel transform is self-reciprocal, that is, the inverse Hankel transform is also given by Definition 2.6.*

Proof. The Hankel transform is self-reciprocal

$$\begin{aligned}
\iff f(s) &= \int_0^\infty (\mathscr{H}_\nu f)(\sigma) J_\nu(s\sigma) \sigma \, d\sigma \\
\iff &= \int_0^\infty \int_0^\infty f(s') J_\nu(s\sigma) s' \, ds' J_\nu(s\sigma) \sigma \, d\sigma \\
&= \int_0^\infty f(s') s' \int_0^\infty J_\nu(s'\sigma) J_\nu(s\sigma) \sigma \, d\sigma \, ds' \\
&= f(s),
\end{aligned}$$

by the orthogonality of the Bessel functions. □

However, only the order zero Hankel transform will be used in the analysis, so the ν shall be omitted and assumed zero, unless otherwise stated. Note that the kernel function of the Hankel transform is not $J_0(s\sigma)s$, but in fact $\sqrt{s}J_0(s\sigma)$, the other $\sqrt{s}$ factor gets absorbed into f. This is to ensure uniform continuity of the kernel (Lemma 2.8), and the continuity of the transform, while minimizing the constraint on f. As a consequence, we have the modified condition that $\int_0^\infty \sqrt{s}|f(s)|ds < \infty$.

Lemma 2.8. *$\sqrt{s}J_0(s\sigma)$ is uniformly continuous on $[0, \infty)$.*

Proof. Let N be a sufficiently large number. By Theorem 2.4, $\sqrt{s}J_0(s\sigma)$ is uniformly continuous on $[0, N]$. And on the interval (N, ∞),

$$J_0(s\sigma) \to \sqrt{\frac{2}{\pi s\sigma}} \cos\left(s\sigma - \frac{\pi}{4}\right)$$

asymptotically, and therefore $\sqrt{s}J_0(s\sigma)$ is uniformly continuous on $[0, \infty)$ since cosine is uniformly continuous everywhere by its periodicity. □

Theorem 2.9. *The Hankel transform is continuous if $\int_0^\infty \sqrt{s}|f(s)|ds < \infty$.*

Proof. Lemma 2.8 shows the uniform continuity of the kernel, and $\int_0^\infty \sqrt{s}|f(s)|ds < \infty$ is a stronger condition than $\int_0^\infty |f(s)|ds < \infty$, thus by Theorem 2.5, the Hankel transform is continuous. □

The following, and final theorem will be particularly useful for calculating the energy deposited to the neutron star.

Theorem 2.10. *The integral of the square of the Hankel transform weighted by σ is equivalent to the integral of the square of the function weighted by s:*

$$\int_0^\infty (\mathscr{H}_\nu f)^2(\sigma)\sigma\, d\sigma = \int_0^\infty f^2(s) s\, ds.$$

Proof. From the definition of the Hankel transform we have

$$\begin{aligned}\int_0^\infty (\mathscr{H}_\nu f)^2(\sigma)\sigma\, d\sigma &= \int_0^\infty \int_0^\infty f(s) J_\nu(s\sigma) s\, ds \int_0^\infty f(s') J_\nu(s'\sigma) s'\, ds'\, \sigma\, d\sigma, \\ &= \int_0^\infty \int_0^\infty f(s) f(s') s\, s' \int_0^\infty J_\nu(s\sigma) J_\nu(s'\sigma)\sigma\, d\sigma\, ds\, ds', \\ &= \int_0^\infty f^2(s) s\, ds\end{aligned}$$

by the orthogonality of Bessel functions. □

2.1.1 Applications of the Hankel Transform

As previously noted, the Hankel transform arises from axisymmetric problems in cylindrical coordinates from the radial eigenfunction of Laplace's equation. Because of this, the Hankel transform along with the Laplace transform have many applications in solving partial differential equations in physics. Some examples include, but are not limited to, the free vibration of a circular membrane, the diffusion equation, acoustic radiation, or even the axisymmetric Cauchy-Poisson wave problem which shares many similarities with this work [8].

3. ANALYTIC SOLUTION

Typically in fluid dynamics, the scalar function known as the velocity potential denoted by φ, is the desired quantity. Once the velocity potential is known, the system is essentially solved because $\vec{\nabla}\varphi = \vec{u}$, and in the case of a free surface, the deformation of the surface can readily be found from the velocity potential as well. The velocity potential will be found in the coming sections, along with the profile of the surface, and lastly the energy deposited into the neutron star will be calculated.

3.1 Eigenfunctions of the Laplacian

The first step in analytically solving for the velocity potential will be to find the eigenfunctions of Laplace's equation, $\nabla^2\varphi = 0$, since the velocity potential is conservative. Since this is a partial differential equation we will assume the solution is the product of univariate functions, $\varphi = f(r)g(\theta)h(z)T(t)$. Expanding the Laplacian for cylindrical systems gives

$$\frac{1}{r}\frac{\partial}{\partial r}\left(r\frac{\partial\varphi}{\partial r}\right) + \frac{1}{r^2}\left(\frac{\partial^2\varphi}{\partial\theta^2}\right) + \frac{\partial^2\varphi}{\partial z^2} = 0.$$

The temporal component can be divided out since the Laplacian does not involve time and will be found later on. Substituting in our assumed form, and dividing by

φ, yields

$$\frac{1}{fr}\frac{\partial}{\partial r}(rf') + \frac{1}{r^2}\frac{g''}{g} + \frac{h''}{h} = 0, \tag{3.1}$$

where primes denote the derivative with respect to the function's only variable. Notice that the function $h(z)$ has been separated from both $f(r)$, and $g(\theta)$, and since each function is univariate, it must be the case that the last term is constant –

$$\frac{h''}{h} = k^2.$$

We cleverly force this constant to be positive to satisfy the boundary conditions, namely, that $h(-\infty) = 0$. The most general solution to this is of course exponentials –

$$h(z) = Ae^{kz} + Be^{-kz}.$$

Since the velocity potential has to vanish at negative infinity, this is simplified to

$$h(z) = e^{kz}, \tag{3.2}$$

without loss of generality we can assume the constant is one since it can be absorbed into $T(t)$. By substituting in k^2 and multiplying through by r^2, (3.1) becomes

$$\frac{r}{f}\frac{\partial}{\partial r}(rf') + k^2r^2 + \frac{g''}{g} = 0, \tag{3.3}$$

and once again, $g(\theta)$ has been separated from $f(r)$, and so the last term must be

constant –

$$\frac{g''}{g} = -\mu^2.$$

The constant is forced to be negative since $g(\theta)$ is expected to be periodic and not exponential. Of course, the general solution to this differential equation is

$$g(\theta) = A\sin(\mu\theta) + B\cos(\mu\theta).$$

However, our system is cylindrically symmetric; there is no way to differentiate one value of θ to another, thus, it is expected that φ has no θ dependence, and consequentially, $g(\theta)$ must be constant, the only way this is satisfied is if $\mu = 0$, so that

$$g(\theta) = 1. \tag{3.4}$$

By substituting $\mu = 0$ into (3.3), and multiplying through by f we obtain

$$r\frac{\partial}{\partial r}(rf') + (k^2r^2 - 0^2)f = 0,$$

which is indeed Bessel's differential equation of order 0. Therefore,

$$f(r) = AJ_0(kr) + BY_0(kr),$$

but, once again, B must equal zero since $Y_0(0)$ is not finite which is unphysical. The

radial part thus simplifies to

$$f(r) = J_0(kr). \tag{3.5}$$

By combining (3.2), (3.4), and (3.5) we find that the velocity potential is

$$\varphi \propto e^{kz} T(t;k) J_0(kr),$$

where k is the eigenvalues. Clearly though, all non-negative, real values of k are a valid solution to Laplace's equation and the boundary conditions. Therefore, the total solution must be the sum of all of these, or since k is valid within an interval, we have the integral form

$$\varphi = \int_0^\infty e^{kz} T(t;k) J_0(kr) dk. \tag{3.6}$$

The temporal component can be solved for using equations of fluid dynamics.

3.2 Temporal Component of the Velocity Potential

The time component of the velocity potential comes from our specific problem. In our case by linearizing and assuming the waves have a small amplitude, we have

$$\left(\frac{\partial \varphi}{\partial t} + (g\eta + \Phi) \right) \Big|_{z=0} = 0,$$

where η denotes the deformation of the surface. This comes from the pressure condi-

tion at the surface [1], and in our case, has the addition of the gravitational potential of the primordial black hole, (1.1). By taking the time derivative and using the relation that

$$\frac{\partial \eta}{\partial t} = \frac{\partial \varphi}{\partial z} \tag{3.7}$$

on the surface [1], we obtain

$$\left(\frac{\partial^2 \varphi}{\partial t^2} + g \frac{\partial \varphi}{\partial z} + \frac{\partial \Phi}{\partial t} \right) \Bigg|_{z=0} = 0. \tag{3.8}$$

In order to solve this partial differential equation, we must write the gravitational potential as an infinite sum of Bessel functions to match the form of φ. We can do so using the Hankel transform using the fact that it is self-reciprocal,

$$\begin{aligned} \frac{\partial \Phi}{\partial t}\bigg|_{z=0} &= \int_0^\infty \left(\mathscr{H} \, \frac{\partial \Phi}{\partial t}\bigg|_{z=0} \right)(k) J_0(kr) k \, dk, \\ &= Gmv^2 t \int_0^\infty \left(\mathscr{H} \, \frac{1}{(r^2 + v^2 t^2)^{3/2}} \right)(k) J_0(kr) k \, dk.^{\S} \end{aligned}$$

Applying the Hankel transform [8, 13] gives

$$\begin{aligned} \frac{\partial \Phi}{\partial t}\bigg|_{z=0} &= Gmv^2 t \int_0^\infty \frac{1}{|vt|} e^{-k|vt|} J_0(kr) k \, dk, \\ &= Gmv \, \mathrm{sgn}(t) \int_0^\infty e^{-kv|t|} J_0(kr) k \, dk, \end{aligned}$$

[§]Note that $\int_0^\infty \sqrt{r}(r^2 + v^2 t^2)^{-3/2} dr = \Gamma^2(3/4)(\pi v^3 t^3)^{-1/2} < \infty$ for $t \neq 0$ which is not concerning since this is true almost everywhere, and so the condition in Theorem 2.5 is satisfied.

which we can now substitute into (3.8) to obtain

$$\int_0^\infty J_0(kr)\ddot{T}(t;k)dk + g\int_0^\infty kJ_0(kr)T(t;k)dk + Gmv\int_0^\infty \operatorname{sgn}(t)e^{-kv|t|}J_0(kr)k\,dk = 0,$$
$$\text{or, } \int_0^\infty \left[\frac{\ddot{T}(t;k)}{k} + gT(t;k) + Gmv\operatorname{sgn}(t)e^{-kv|t|}\right] J_0(kr)k\,dk = 0.$$

But, this is nothing more than the Hankel transform of the differential equation for T. By taking the Hankel transform of both sides we can remove the integral, giving an ordinary differential equation for the time component:

$$\frac{\ddot{T}(t;k)}{k} + gT(t;k) + Gmv\operatorname{sgn}(t)e^{-kv|t|} = 0.$$

Clearly, the homogeneous solution is $T(t;k) = A\cos(\omega_k t) + B\sin(\omega_k t)$ with $\omega_k^2 = gk$.

The form of this differential equation suggests the particular solution should take the form $T(t;k) = Ce^{-kv|t|}$. Substituting this in yields

$$C\left(k^2v^2\operatorname{sgn}^2(t)e^{-kv|t|} + gke^{-kv|t|}\right) + Gmvk\operatorname{sgn}(t)e^{-kv|t|} = 0.$$

Now, by rearranging we find

$$\begin{aligned} C &= \frac{-Gmvk\operatorname{sgn}(t)}{k^2v^2 + gk}, \\ &= \frac{Gmv}{g}\frac{-\operatorname{sgn}(t)}{1 + kv^2/g} \end{aligned}$$

as the coefficient, and,

$$T(t;k) = \frac{Gmv}{g}\frac{1}{1 + kv^2/g}\left(-\operatorname{sgn}(t)e^{-kv|t|}\right) + A\cos(\omega_k t) + B\sin(\omega_k t)$$

as the full time component of the velocity potential. We can now apply the boundary conditions to find A, and B. Physically, we expect $T(t;k) \in C^1(-\infty,\infty)$, furthermore, we only expect the sinusoidal terms to contribute at times greater than zero, thus finally, we procure

$$\begin{aligned} T(t;k) &= \frac{Gmv}{g}\frac{1}{1+kv^2/g}\left(-\operatorname{sgn}(t)e^{-kv|t|}+2H(t)\cos(\omega_k t)\right), \text{ and,} \\ \varphi &= \frac{Gmv}{g}\int_0^\infty \frac{J_0(kr)e^{kz}}{1+kv^2/g}\left(-\operatorname{sgn}(t)e^{-kv|t|}+2H(t)\cos(\omega_k t)\right)dk. \end{aligned}$$

Another way the velocity potential can be expressed is as the Hankel transform of its time component, $\varphi = \left(\mathscr{H}\, e^{kz}\frac{T(t;k)}{k}\right)(r,z,t)$; this will be of particular importance in Section 3.4 for the energy calculation.

3.3 Deformation of the Surface

Now that the velocity potential has been acquired, naturally the next step is to find the shape of the surface waves – η. This can easily be done by integrating both sides of (3.7) so that

$$\eta = \int_0^t \left.\frac{\partial\varphi}{\partial z}\right|_{z=0} dt.$$

It is now just a matter of taking the partial derivative and integrating:

$$\begin{aligned} \eta &= \frac{Gmv}{g}\int_0^\infty \frac{kJ_0(kr)}{1+kv^2/g}\left(\int_0^t -\operatorname{sgn}(t)e^{-kv|t|}+2H(t)\cos(\omega_k t)\,dt\right)dk, \\ &= \frac{Gm}{g}\int_0^\infty \frac{J_0(kr)}{1+kv^2/g}\left(e^{-kv|t|}+2H(t)v\sqrt{\frac{k}{g}}\sin(\omega_k t)\right)dk. \end{aligned} \tag{3.9}$$

As with the velocity potential it will be convenient to express this as a Hankel transform, specifically,

$$\eta = \left(\mathscr{H} \frac{\widetilde{T}(t;k)}{k} \right)(r,t),$$

where

$$\widetilde{T}(t;k) = \frac{Gm}{g} \frac{1}{1+kv^2/g} \left(e^{-kv|t|} + 2H(t)v\sqrt{\frac{k}{g}} \sin(\omega_k t) \right)$$

is the time component of η.

It is useful to nondimensionalize (3.9) to get a better idea of the scaling of the surface waves instead of for a specific scenario. By making the substitutions

$$\kappa = \frac{v^2}{g}k, \quad \chi = \frac{g}{v^2}r, \quad \tau = \frac{g}{v}t,$$

then,

$$\eta = \frac{Gm}{v^2} \int_0^\infty \frac{J_0(\kappa\chi)}{1+\kappa} \left(e^{-\kappa|\tau|} + 2H(\tau)\sqrt{\kappa}\sin(\omega_\kappa \tau) \right) d\kappa,$$

with $\omega_\kappa^2 = \kappa$.

This expression for the surface waves can be numerically integrated (the results can be found in Figure 3.1). Initially before the collision, the primordial black hole causes the surface of the neutron star to rise. At impact, a large wave is created which slowly decays as it traverses outwards. After which waves of smaller and smaller wavelength are observed slowly moving away from the point of impact.

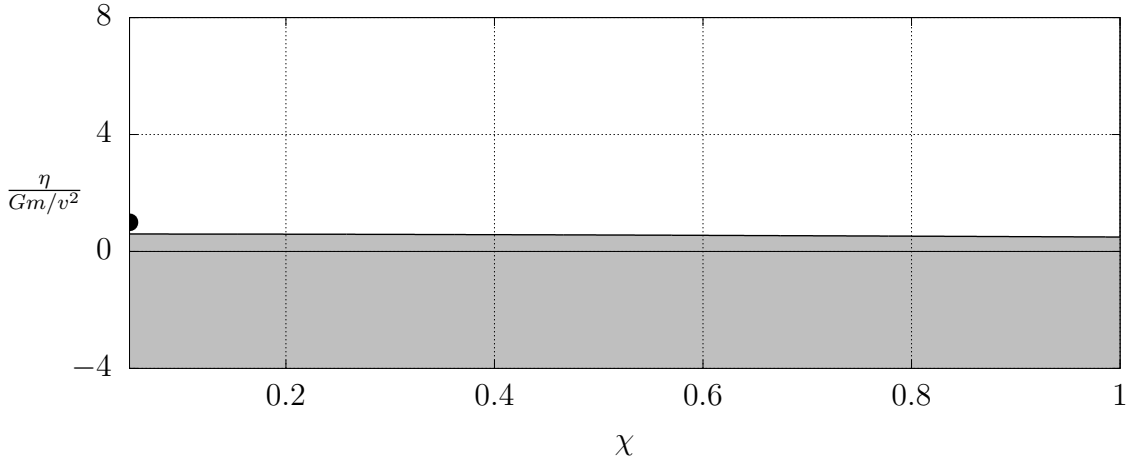

(a) $\tau = -1$

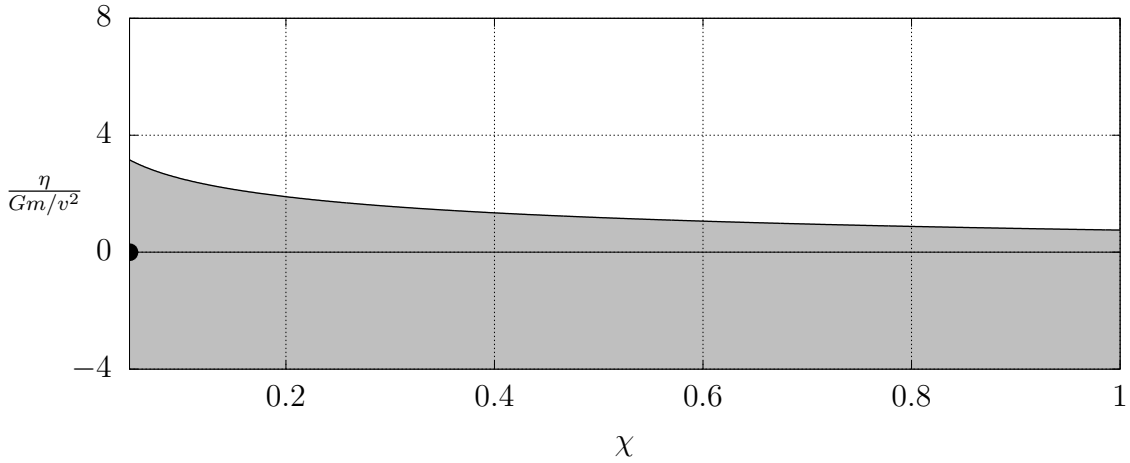

(b) $\tau = 0$

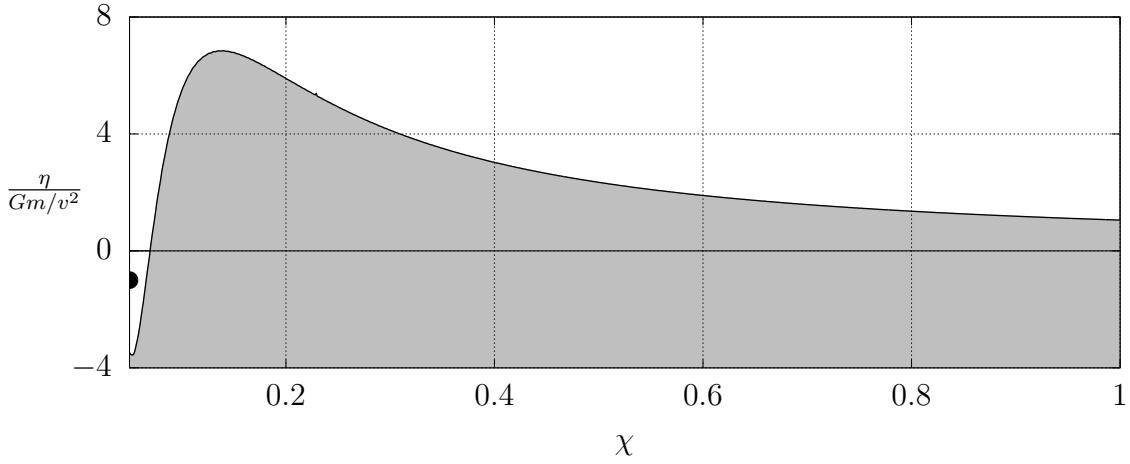

(c) $\tau = 1$

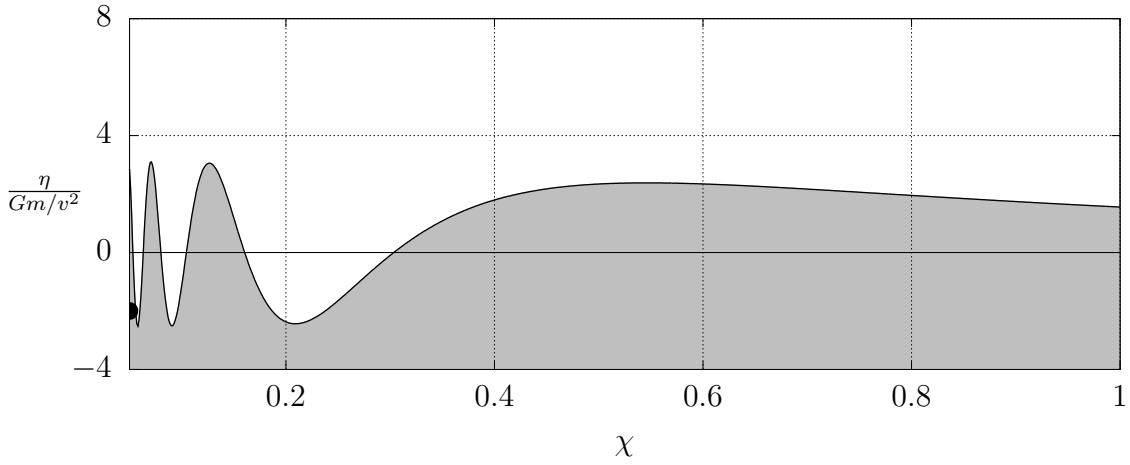

(d) $\tau = 2$

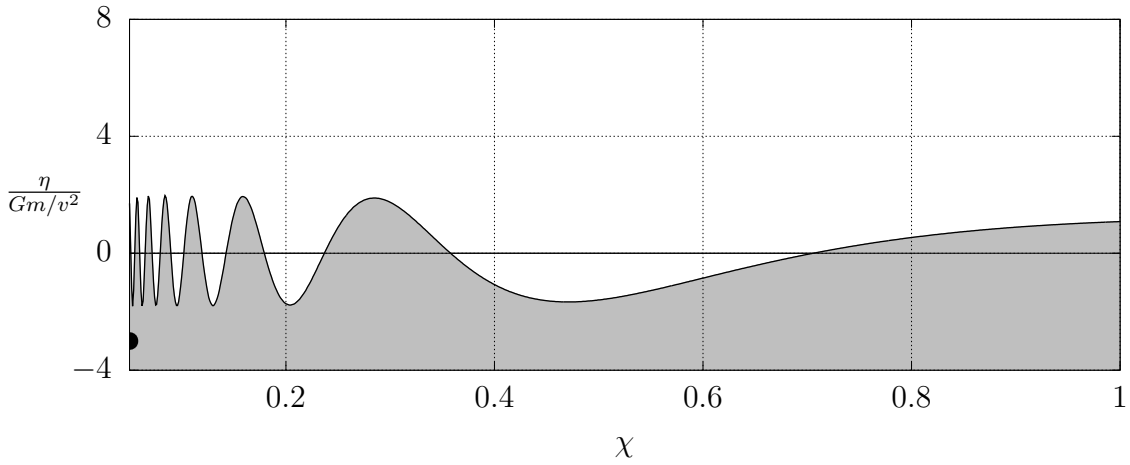

(e) $\tau = 3$

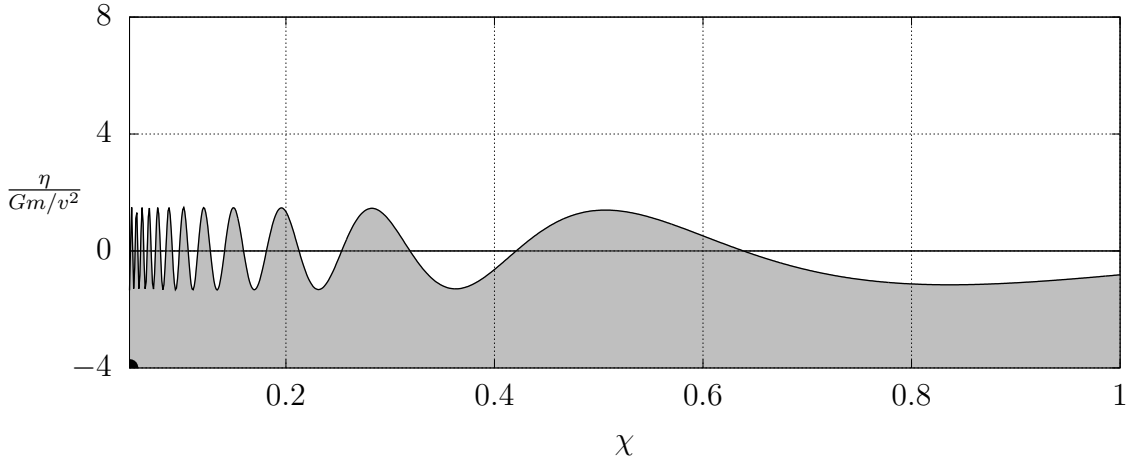

(f) $\tau = 4$

Figure 3.1: Deformation of the surface of a neutron star around the time of impact. The full animation can be found at `https://github.com/bmetherall/Primordial_Black_Holes/blob/master/Videos/AnalyticWaves.gif`.

3.4 Calculating the Energy Transferred

Finally, the last quantity of interest is the energy. Having an idea of what the waves would look like is great, however, if such a collision were to take place, the waves would not be detectable from Earth. On the other hand, the energy would. Clearly, in order to make reasonable predictions about what may be detected on Earth more than just Newtonian gravity is necessary. Since energy does not escape the system in this model (it is only transferred between the primordial black hole and the neutron star) predictions cannot be made about what such an event would look like from Earth, but it is a worthwhile calculation nonetheless.

To calculate the energy transferred we shall start with

$$E(t) = \frac{1}{2}\rho \int_V \left|\vec{\nabla}\,\varphi\right|^2 + \rho g \int_V z,$$

where $\vec{\nabla}\,\varphi$ is of course $\vec{u}$, which is a typical expression for energy, except we use the density of a fluid element instead of its mass. We can expand the volume integrals out so that

$$E(t) = \frac{1}{2}\rho \int_0^{2\pi}\int_0^{\infty}\int_{-\infty}^{0} \left|\vec{\nabla}\,\varphi\right|^2 dz\, r\, dr\, d\theta + \rho g \int_0^{2\pi}\int_0^{\infty}\int_0^{\eta} z\, dz\, r\, dr\, d\theta.$$

Notice that the bounds on z for the potential energy are from 0 to η. This is because we are interested in the change in energy so we subtract the initial potential energy of the neutron star. After solving the trivia integrals we find that

$$E(t) = \rho\pi \left(\int_0^{\infty}\int_{-\infty}^{0} \left(\frac{\partial\varphi}{\partial r}\right)^2 r\, dz\, dr + \int_0^{\infty}\int_{-\infty}^{0} \left(\frac{\partial\varphi}{\partial z}\right)^2 r\, dz\, dr + g\int_0^{\infty} \eta^2 r\, dr \right).$$

These are non-trivial integrals since φ, and η are themselves non-trivial integrals. To simplify and tidy this calculation, let ♣, ♠, and ♦ be the three terms respectively, so that $E = \rho\pi(\clubsuit + \spadesuit + g\diamondsuit)$.

The reason we wrote the velocity potential, and the deformation of the surface as the Hankel transform of their time components is so these integrals can more easily be solved with the aid of Theorem 2.10. Starting with the first term,

$$\clubsuit = \int_0^\infty \int_{-\infty}^0 \left(\frac{\partial \varphi}{\partial r}\right)^2 r\, dz\, dr,$$

$\partial\varphi/\partial r$ can be replaced by its Hankel transform representation so that

$$\clubsuit = \int_{-\infty}^0 \int_0^\infty \left(\mathscr{H}_1\, e^{kz} T(t;k)\right)^2 (r,z,t) r\, dr\, dz,$$

and after invoking Theorem 2.10

$$\clubsuit = \int_{-\infty}^0 \int_0^\infty e^{2kz} T^2(t;k)\, k\, dk\, dz,$$

then by integrating over z we get the final expression

$$\clubsuit = \frac{1}{2} \int_0^\infty T^2(t;k)\, dk.$$

Following this same procedure for the other two terms we find that

$$\spadesuit = \frac{1}{2} \int_0^\infty T^2(t;k)\, dk, \text{ and}$$
$$\diamondsuit = \int_0^\infty \frac{\widetilde{T}^2(t;k)}{k}\, dk.$$

Combining these we find

$$E(t) = \rho\pi \int_0^\infty T^2(t;k) + g\frac{\widetilde{T}^2(t;k)}{k}\, dk,$$

which after expanding out in full

$$E(t) = \frac{G^2m^2\rho\pi}{g}\int_0^\infty \frac{v^2}{g}\left(\frac{-\operatorname{sgn}(t)e^{-kv|t|} + 2\,\mathrm{H}(t)\cos(\omega_k t)}{1+kv^2/g}\right)^2 + \frac{1}{k}\left(\frac{e^{-kv|t|} + 2\,\mathrm{H}(t)v\sqrt{\frac{k}{g}}\sin(\omega_k t)}{1+kv^2/g}\right)^2 dk.$$

Using the same substitutions as before, we can nondimensionalize the energy

$$E(\tau) = \frac{G^2m^2\rho\pi}{g}\int_0^\infty \left(\frac{-\operatorname{sgn}(\tau)e^{-\kappa|\tau|} + 2\,\mathrm{H}(\tau)\cos(\omega_\kappa \tau)}{1+\kappa}\right)^2 + \frac{1}{\kappa}\left(\frac{e^{-\kappa|\tau|} + 2\,\mathrm{H}(\tau)\sqrt{\kappa}\sin(\omega_\kappa \tau)}{1+\kappa}\right)^2 dk. \tag{3.10}$$

Figure 3.2 shows a plot of the energy for times near the collision. Initially, the energy grows exponentially, then at $\tau = 0$, when the primordial black hole collides with the neutron star, a considerable amount of energy is deposited. After which a majority of the energy is carried away exponentially by the primordial black hole. The long time limit is perhaps more useful since that is the net energy transfer of the interaction. By taking the limit as $\tau \to \infty$ of (3.10), the exponential terms decay to zero, and the sine and cosine simplify to 1. This new integrand has an elementary antiderivative, and so after integrating, the energy becomes

$$E = 4\pi\rho\frac{G^2m^2}{g} \tag{3.11}$$

which is a surprisingly compact form.

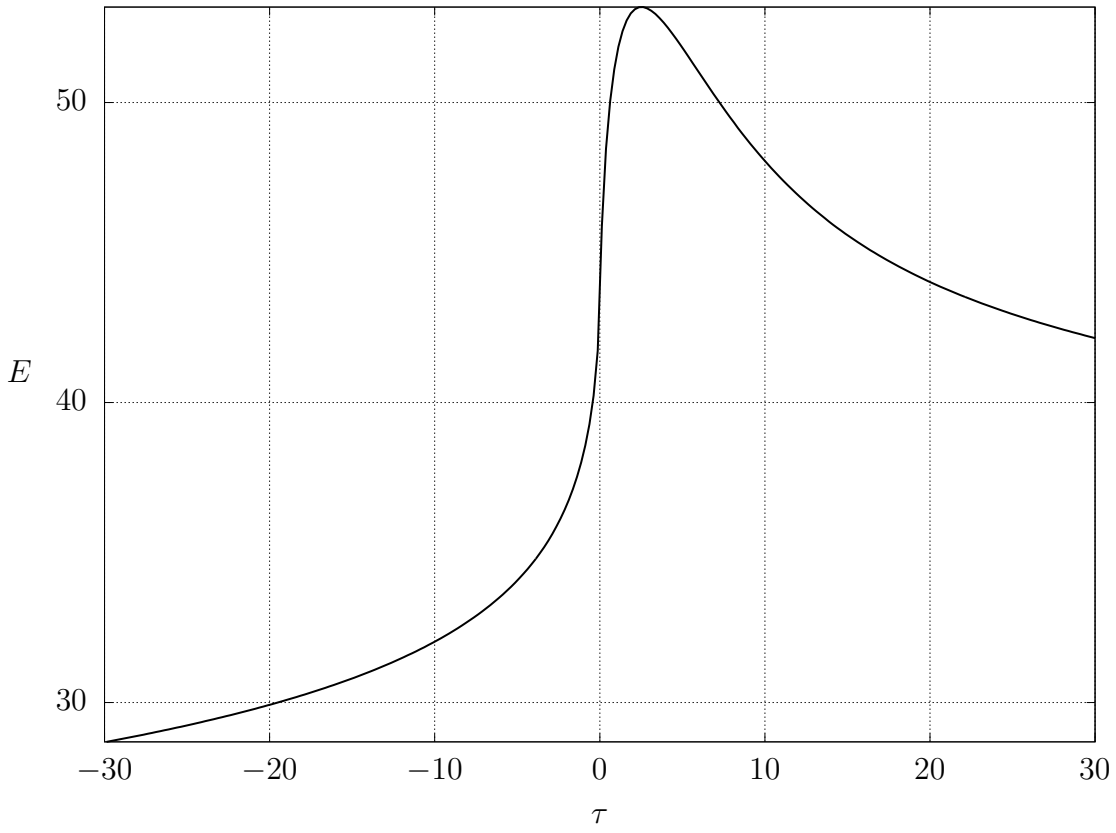

Figure 3.2: Energy transfer of the interaction for short times; with units of energy of $\frac{G^2 m^2 \rho \pi}{g}$.

The dynamical friction approach [3] finds that the energy loss is

$$E = \frac{4G^2m^2M}{R^2}\left\langle \frac{\ln\Lambda}{v^2} \right\rangle,$$

where the logarithmic term is the Coulomb logarithm, which in the case of typical stars is approximately 30. We can compare this to our answer by assuming the average velocity is on the order of the escape velocity

$$\left\langle v^2 \right\rangle = \frac{2GM}{R},$$

and by using the usual form for gravitational acceleration. Then, our expression for the energy can then be simplified to

$$E = \frac{3Gm^2}{R},$$

and the dynamical friction expression to

$$E = \frac{2Gm^2}{R}\ln\Lambda$$

which agrees to within around an order of magnitude.

4. SIMULATION SOLUTION

4.1 Smoothed Particle Hydrodynamics

Since we model neutron stars as a fluid, in order to simulate the collision of a primordial black hole with a neutron star, we need to use computational fluid dynamics, more specifically, smoothed particle hydrodynamics. Smoothed particle hydrodynamics was initially developed in 1977 for simulating spherically asymmetric stars [12]. A major assumption in the modelling of stars is that they are spherically symmetric, however, there are a lot of cases where this is not true. For example the collapse of a protostar will be very inhomogeneous; or if the star has a large angular momentum / strong magnetic fields, the star will be considerably deformed [12].

Smoothed particle hydrodynamics has since been extended more generally so it can be applied outside of astrophysics such as solid mechanics, and fluid dynamics. In essence, smoothed particle hydrodynamics uses similar methods of N-body code – the continuous media is represented as a set of particles, and the equations are solved numerically. Mathematically, the particles represent the points at which the properties of the fluid are calculated, the rest can then be interpolated. Physically, the particles are simply a subset of all the particles in the system [17]. One of the biggest advantages of smoothed particle hydrodynamics is that it is mesh-free, unlike most computational fluid dynamics methods. Therefore, it is very useful for interactions

between different types of particles, and for free surface simulations.

Typically, smoothed particle hydrodynamics uses a nearest neighbour scheme for calculating the changes in a particle's properties. This is done by using a cubic Hermite spline to interpolate properties within a radius of twice the smoothing length of a particular particle. A cubic Hermite spline is a set of cubic polynomials specified by its values, and the values of its first derivative at the boundaries of the interval.

4.1.1 PySPH

The simulations were conducted with PySPH [20]; open source SPH code written in Python and compiled in Cython. This allows a majority of the code to be written in pure Python, but is then converted to high performance Cython code to run at speeds closer to C and FORTRAN. For further optimizations, PySPH can run in parallel with OpenMP and MPI to take advantage of multiple cores / threads. One of the main reasons for choosing PySPH is that it allows user defined classes, and equations which was needed to incorporate the primordial black hole.

4.2 Code

In order to simulate a primordial black hole collision with a neutron star we must first write a class to include the acceleration. The acceleration of course is just

$$\vec{a} = -\frac{1}{m_{part}} \vec{\nabla} \Phi.$$

Within the coordinates in PySPH

$$\vec{a} = \frac{-m}{\left(x^2 + s^2 + (y + v\tau)^2\right)^{3/2}} \begin{pmatrix} x \\ y + v\tau \end{pmatrix}$$

with $G = 1$, $\tau = t - t\_hit$, and s a softening length so the solution does not diverge at $\tau = 0$ at the origin. The mass of the particle is also omitted in the simulation because PySPH uses acceleration per unit mass. In the class function (Figure 4.1) the velocity is hard coded to be 1, and the parameter *t_hit* is used to offset the collision of the primordial black hole since the simulation starts at $t = 0$.

Now that the class function has been written, it can be called within the equations block of the main file, *blackhole.py*. Figure 4.2 shows the important sections of *blackhole.py*; first the acceleration equation is imported, and the values for the simulation are specified in the preamble. Then, the black hole can be added to the equations group in the main acceleration block. The included example *hydrostatic_tank.py* was used as the base for *blackhole.py*, it was the most useful starting point – it is a 2D tank filled with fluid, and includes the force of gravity.

The parameters of the simulation were mostly the same as what were used to generate the images of the analytic solution – everything set equal to unity – with the exceptions of $t\_hit = 200$, and $s = 0.01$. The reason *t_hit* is so large is due to how the particles are initially placed. They are simply placed on a grid with spacing dx; once the simulation starts, gravity pulls the surface down attempting to equilibrate to a linear pressure gradient. However, since the fluid is not at equilibrium, the surface undergoes harmonic motion and is slowly dampened to equilibrium and so the long *t_hit* is an attempt to dampen out a majority of the oscillations.

```
1 from pysph.sph.equation import Equation
2
3 class BlackHole2D(Equation):
4     def __init__(self, dest, sources, soft=0.05, t_hit=5.0, M
    =1.0):
5         self.soft = soft # softening length to not divide by
    zero
6         self.t_hit = t_hit # time when the black hole crosses
     the origin
7         self.M = M # mass of black hole
8         super(BlackHole2D, self).__init__(dest, sources)
9
10     def initialize(self, d_idx, d_au, d_av):
11         d_au[d_idx] = 0.0
12         d_av[d_idx] = 0.0
13
14     # calculate the force due to the black hole
15     def loop(self, d_x, d_y, d_idx, d_au, d_av, t):
16         d_au[d_idx] += -self.M * d_x[d_idx] / pow((d_x[d_idx
    ]**2 + self.soft**2 + (d_y[d_idx] + t - self.t_hit)**2)
    ,3.0/2.0)
17         d_av[d_idx] += -self.M * (d_y[d_idx] + t - self.t_hit
    ) / pow((d_x[d_idx]**2 + self.soft**2 + (d_y[d_idx] + t -
    self.t_hit)**2),3.0/2.0)
```

Figure 4.1: Class file for adding the acceleration due to the primordial black hole, *BlackHoleEquation.py*.

```
19 # Import the equations
20 from pysph.sph.equation import Group
21 from pysph.sph.BlackHoleEquation import BlackHole2D

40 # Domain and reference values
41 Lx = 120.0; H = 15.0; Ly = 1.5*H
42 gy = -1.0
43 Vmax = np.sqrt(abs(gy) * H)
44 c0 = 10 * Vmax; rho0 = 1.0
45 p0 = c0*c0*rho0
46 gamma = 1.0
47
48 soft = 0.01
49 t_hit = 200.0
50 Mass = 1.0
51 tf = 300.0
52
53 # Reynolds number and kinematic viscosity
54 Re = 0; nu = 0.01 # Ideal fluid
55
56 # Numerical setup
57 nx = 1600; dx = Lx/nx
58 ghost_extent = 5.5 * dx
59 hdx = 1.2

82 class BlackHole(Application):

171     def create_equations(self):
172         # Formulation for REF1
173         equations1 = [

194             # Main acceleration block
195             Group(equations=[

212                 # Add the black hole
213                 BlackHole2D(dest='fluid', sources=None, soft=
    soft, t_hit=t_hit, M=Mass)
214
215             ]),
216         ]
```

Figure 4.2: Modifications of the hydrostatic tank example, *blackhole.py*.

Determining the dimensions of the tank required a considerable amount of care. If the tank was too narrow, the walls at the edges would reflect the initial waves which would then start to interfere with the secondary waves. This caused erroneous results in the energy calculations during testing. Similarly, if the tank was too shallow, the waves resembled shallow water waves instead of deep, as in our model. And of course, if the tank was needlessly large, it greatly affected the computation time of the simulation. In the end, $Lx = 120$, $Ly = 15$, and $dx = 0.075$ were decided on.

4.3 Simulation Results

In total the simulation took about 330 CPU hours over the course of three days. The resulting surface waves from the collision can be seen in Figure 4.3. As with the analytic results, we see that the surface of the neutron star pulls upwards before the collision due to the gravitational force of the primordial black hole. Then, after the collision, the initial wave propagates outwards. It is fairly difficult to notice, however, a second much smaller amplitude wave is created as well. Unfortunately, because of the resolution of the simulation, waves smaller than dx cannot be seen, unlike in the analytic solution which had a much smaller spacing.

In order to calculate the energy we do so in the traditional way, by taking the sum of the potential and kinetic energies of each particle,

$$\begin{aligned} E &= \sum_i T_i + U_i, \\ &= \sum_i \frac{1}{2} m_i \left(u_i^2 + v_i^2\right) + m_i g y_i. \end{aligned}$$

However, to compare to the analytic result, we must transform this into three dimen-

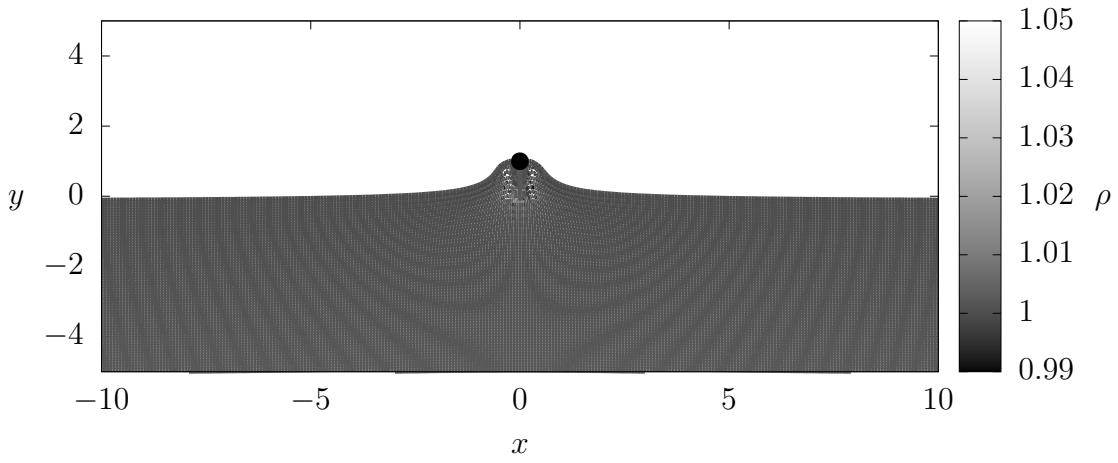

(a) $\tau = -1$

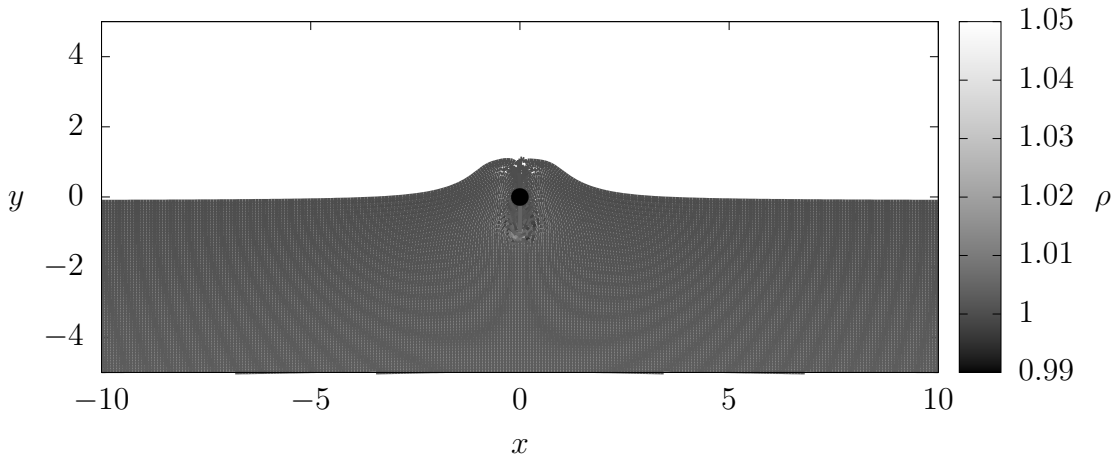

(b) $\tau = 0$

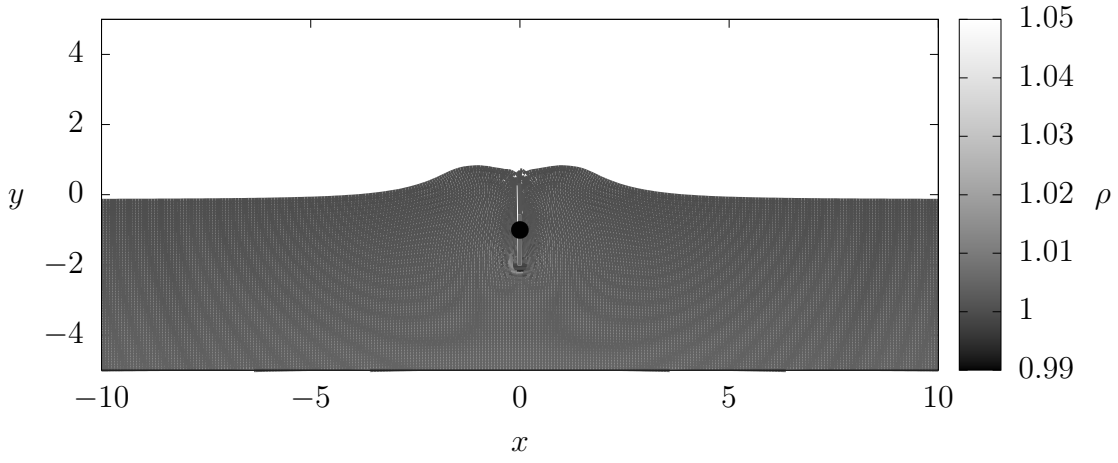

(c) $\tau = 1$

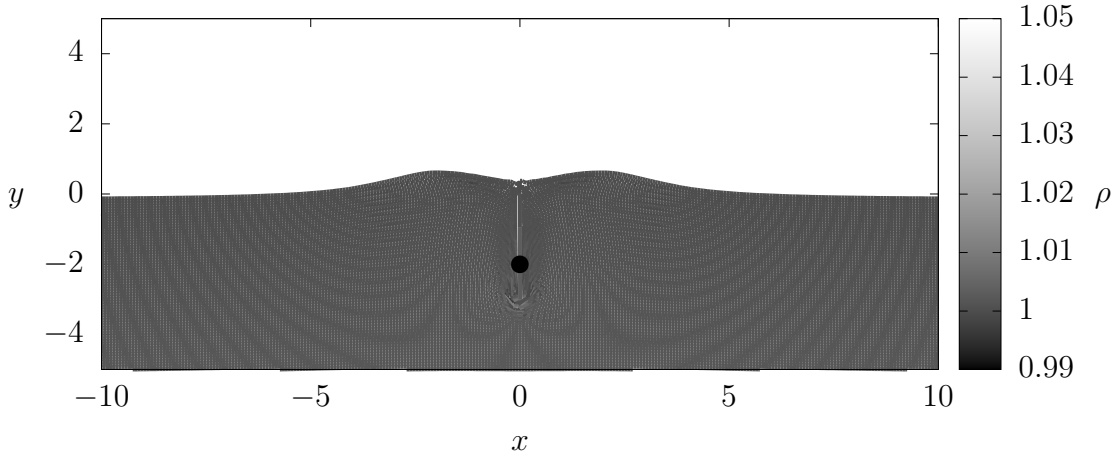

(d) $\tau = 2$

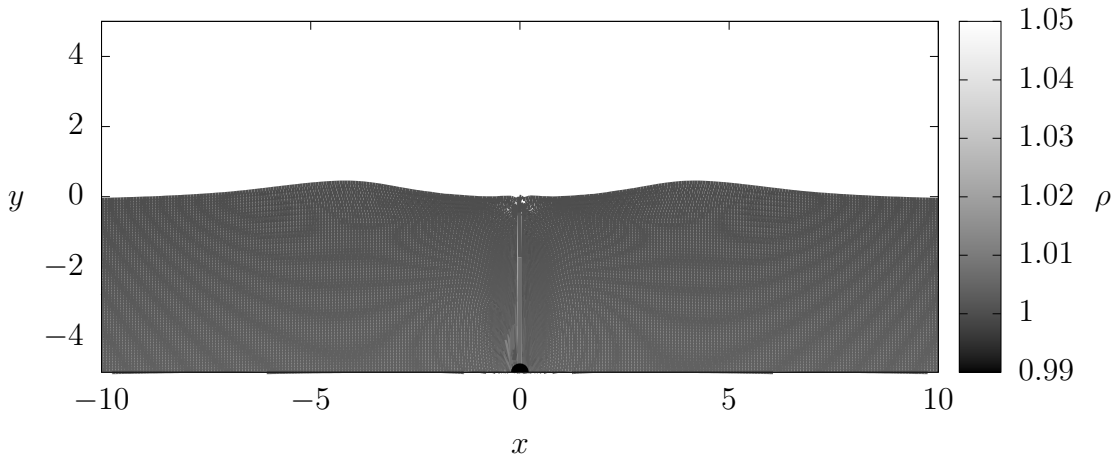

(e) $\tau = 5$

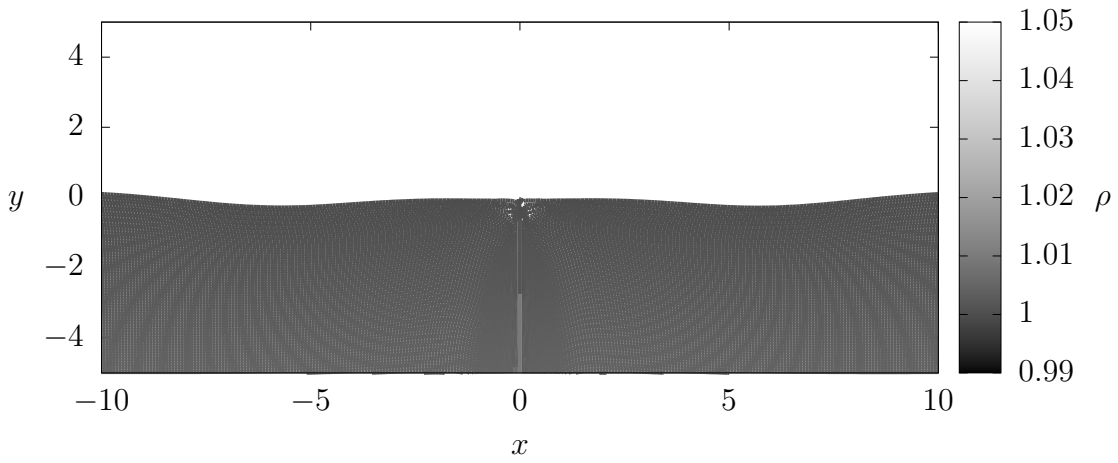

(f) $\tau = 10$

Figure 4.3: Surface waves resulting from the simulation. The full animation can be found at `https://github.com/bmetherall/Primordial_Black_Holes/blob/master/Videos/Simulation.gif`.

sions by revolving about the y axis. This can be done by weighting each particle by $\pi|x_i|/dx$,

$$E = \frac{\pi}{dx} \sum_i \left(\frac{1}{2} \left(u_i^2 + v_i^2 \right) + g y_i \right) m_i |x_i|.$$

This is essentially the same as a shell integration, however, we only integrate through π, and the absolute value of the x coordinate is needed. The energy is calculated in this fashion for all time steps and is plotted in Figure 4.4a. Clearly, this is of little use since the energy is full of noise and highly oscillatory. As mentioned before, this is also the result of how the particles are initially placed within the simulation. As the surface oscillates up and down while attempting to equilibrate, so too does the potential energy. The oscillations have a period of 39 time steps, and therefore, by taking running averages of 39 time steps, most of the noise is removed. Also for clarity, the damping is removed, and the energy has been shifted to start at 0; the resulting plot is much cleaner and is in Figure 4.4b.

This cleaned up energy has a very similar shape to the analytic calculation; initially, the neutron star gains energy as the primordial black hole approaches. And after the collision there is a large peak in the energy similar to the analytic solution. However, this jump in energy is much larger. Furthermore, at approximately $\tau = 40$ the initial wave hits the boundaries which causes the energy of the system to increase as the wave climbs the wall. After this, the wave is reflected back towards the centre of the tank. This also causes the first wave to interfere with the smaller waves trailing it which again causes the energy to increase – this is the main cause of the erratic behaviour of the energy at times greater than 40.

Another point of interest is that since the tank has a depth of 15, at $\tau = 15$ the

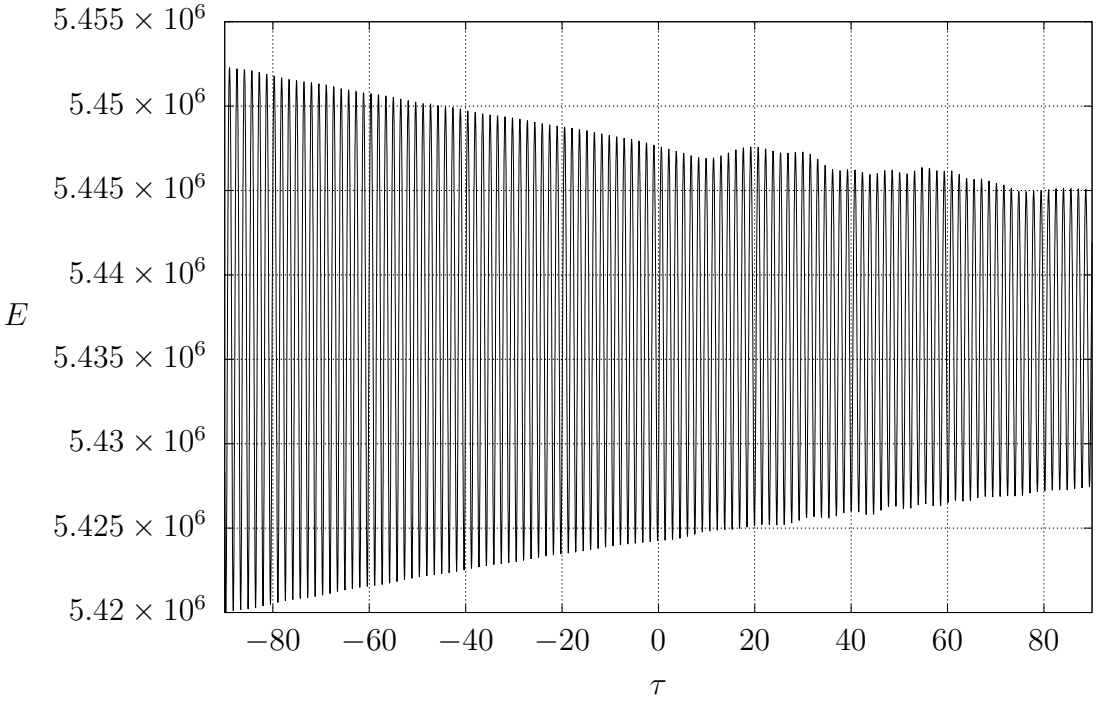

(a) Crazy looking energy.

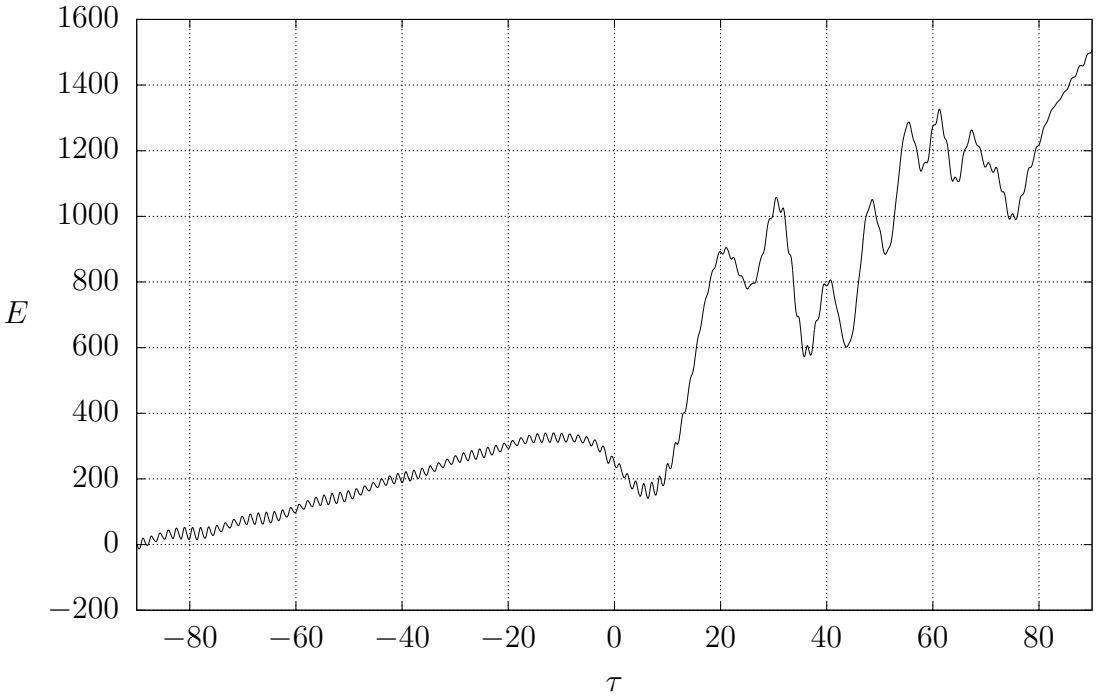

(b) Smoothed energy without noise.

Figure 4.4: Energy transfer from the simulation.

primordial black hole exits the tank. During the lower resolution testing this did not appear to affect the results of the simulation, however, it indeed does. As the primordial black hole exits the tank a shock wave is created. In Figure 4.5 the shock wave can be seen moving outwards from the bottom of the tank, and when it reaches the surface, it is reflected back into the star. Given the speed of the shock wave and the dimensions of the tank, it will be dampened out within a few time units and does not appear to effect the energy of the system.

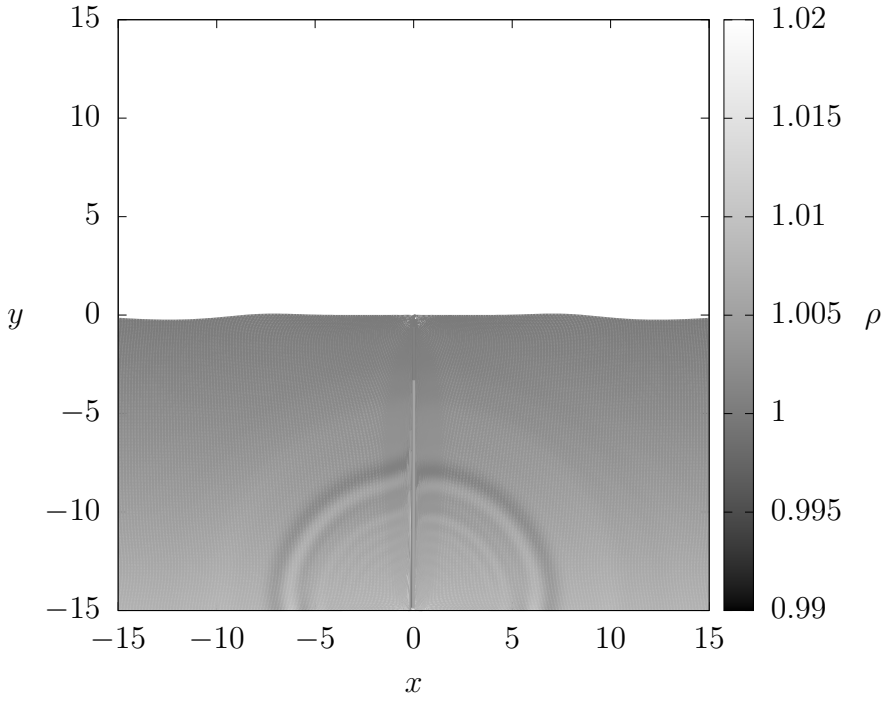

(a) Initial shock-wave. $\tau = 15.24$.

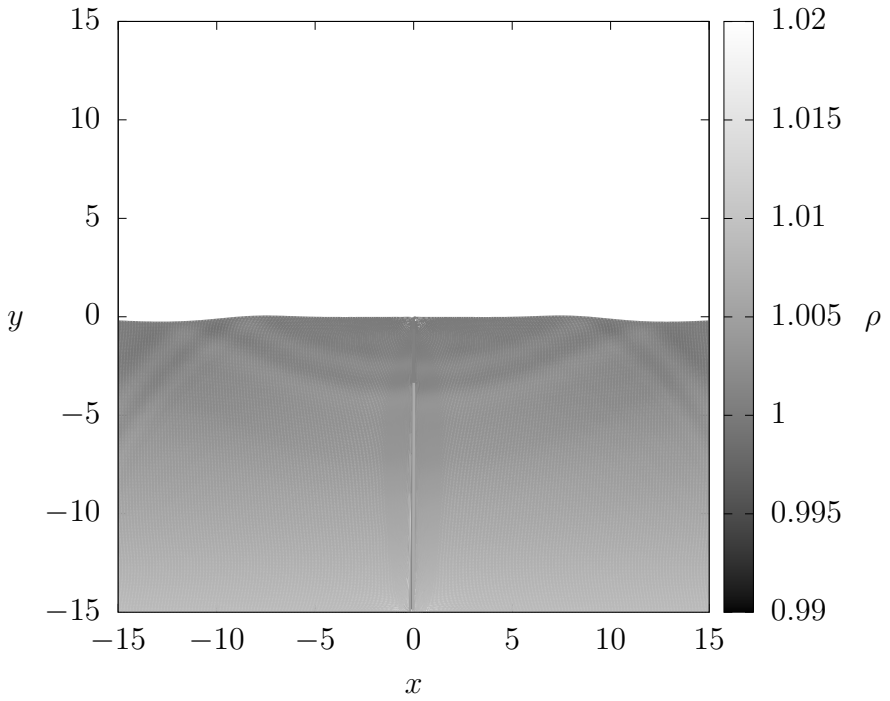

(b) Reflected shock-wave. $\tau = 15.56$.

Figure 4.5: Shock-wave created by primordial black hole leaving tank.

5. CONCLUSIONS

In this thesis we looked at the effect a primordial black hole has on the surface of a neutron star if the primordial black hole were to pass through the neutron star. To simplify the problem we first assume that a neutron star is an infinite plane, and that primordial black holes are point masses. One of the main results was analytically showing that the energy transfer in this model is

$$E = 4\pi\rho\frac{G^2m^2}{g}.$$

We also independently simulated the collision with smoothed particle hydrodynamics. The profile of the energy transfer matched similarly in both cases, however, in the simulation there was several disturbances in the energy skewing the shape.

If we were to further develop this work, there are a few obvious modifications, and extensions. Firstly, there are better methods of simulating the collision so that the fluid is started at equilibrium to stop the oscillations of the surface, and so the walls of the tank do not reflect the waves back into the centre. The next step to improve the result would be moving from an infinite plane to a spherical star, to better match reality. Defillon, Granet, Tinyakov, and Tytgat [9] investigated the spherical case as well, as the flat star, however, within the time constraints of this thesis, it was not looked at in great detail.

Finally, to obtain the most precise estimates of the energy transfer between a primordial black hole and a neutron star – and what may be observed here on Earth – much more sophisticated physics needs to be incorporated. For example, a group in Illinois uses full general relativistic magnetohydrodynamics (GRMHD) code to simulate events such as black hole mergers, or gravitational waves [10].

REFERENCES

[1] D. J. Acheson, *Elementary Fluid Dynamics*, Oxford University Press, 1990.

[2] A. Barrau, D. Blais, G. Boudoul, D. Polarski, *Peculiar Relics from Primordial Black Holes in the Inflationary Paradigm*, Annalen der Physik 13, 2003.

[3] Fabio Capela, Maxim Pshirkov, and Peter Tinyakov, *Constraints on Primordial Black Holes as Dark Matter Candidates from Capture by Neutron Stars*, American Physics Society Phys. Rev. D 87, 2013.

[4] Bernard Carr, Florian Kühnel, and Marit Sandstad, *Primordial Black Holes as Dark Matter*, American Physical Society Phys. Rev. D 94, 2016.

[5] B. J. Carr, and M. Sakellariadou, *Dynamical Constraints on Dark Matter in Compact Objects*, The Astrophysical Journal 516, 1999.

[6] Pierre Cousin, *Sur les Fonctions de n Variables Complexes*, Acta Math. 19, 1895.

[7] Richard H. Cyburt, Brian D. Fields, Keith A. Olive, *Primordial Nucleosynthesis in Light of WMAP*, Harvard Colloquia, 2003.

[8] Lokenath Debnath, and Dambaru Bhatta, *Integral Transforms and Their Applications*, Chapman & Hall/CRC, 2007.

[9] Guillaume Defillon, Etienne Granet, Peter Tinyakov, and Michel H.G. Tytgat, *On Tidal Capture of Primordial Black Holes by Neutron Stars*, American Physics Society Phys. Rev. D 90, 2014.

[10] Zachariah B. Etienne, Vasileios Paschalidis, Roland Hass, Philipp Moesta, Stuart L. Shapiro, *IllinoisGRMHD: An Open-Source, User-Friendly GRMHD Code for Dynamical Spacetimes*, Classical and Quantum Gravity 32, 2015.

[11] Paul H. Frampton, *Searching for Dark Matter Constituents with Many Solar Masses*, World Scientific, 2016.

[12] R. A. Gingold, and J. J. Monaghan, *Smoothed Particle Hydrodynamics: Theory and Application to Non-Spherical Stars*, Monthly Notices of the Royal Astronomical Society 181, 1977.

[13] I. S. Gradshteyn, and I. M. Ryzhik, *Table of Integrals, Series, and Products*, Elsevier Inc., 2007.

[14] D. H. Griffel, *Applied Functional Analysis*, Dover Publishing Inc., 2002.

[15] S. W. Hawking, *Black Hole Explosions?*, Nature, 1974.

[16] G. Jungman, M. Kamionkowski, K. Griest, *Supersymmetric Dark Matter*, Physics Report 267, 1996.

[17] J. J. Monaghan, *Smoothed Particle Hydrodynamics*, Reports on Progress in Physics 68, 2005.

[18] Robert J. Nemiroff, Gabriela F. Marani, Jay P. Norris, Jerry T. Bonnell, *Limits on the Cosmological Abundance of Supermassive Compact Objects from a Millilensing Search in Gamma-Ray Burst Data*, Physical Review Letters 86, 2001.

[19] Paolo Pani, and Abraham Loeb, *Tidal Capture of a Primordial Black Hole by a Neutron Star: Implications for Constrains on Dark Matter*, Journal of Cosmology and Astroparticle Physics, 2014.

[20] Prabhu Ramachandran, *PySPH: a reproducible and high-performance framework for smoothed particle hydrodynamics*, In Proceedings of the 15th Python in Science Conference, 2016.

[21] Barbara Ryden, *Introduction to Cosmology*, Addison Wesley, 2003.

[22] P. Tisserand, et al., *Limits on the Macho Content of the Galactic Halo from the EROS-2 Survey of the Magellanic Clouds*, Astronomy & Astrophysics, 2007.

[23] P. N. Wilkinson, et al., *Limits on the Cosmological Abundance of Supermassive Compact Objects form a Search for Multiple Imaging in Compact Radio Sources*, Physical Review Letters 86, 2001.